Talanta 278 (2024) 126444

Contents lists available at ScienceDirect

Talanta

journal homepage: www.elsevier.com/locate/talanta

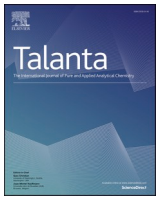

Determination of time since deposition of bloodstains through NIR and UV–Vis spectroscopy – A critical comparison

Sara Gariglio [a,b], Cristina Malegori [a,**], Alicja Menżyk [c,d], Grzegorz Zadora [c,d], Marco Vincenti [e], Monica Casale [a], Paolo Oliveri [a,*]

[a] Department of Pharmacy (DIFAR), University of Genova, Viale Cembrano 4, Genova, Italy
[b] Department of Chemistry and Industrial Chemistry (DCCI), University of Genova, Via Dodecaneso 31, Genova, Italy
[c] Institute of Chemistry, University of Silesia in Katowice, Szkolna 9, Katowice, Poland
[d] Institute of Forensic Research in Krakow, Westerplatte 9, Krakow, Poland
[e] Department of Chemistry, University of Turin, Via Pietro Giuria 7, Torino, Italy

ARTICLE INFO

Keywords:
Bloodstains dating
Near infrared spectroscopy
UV–Vis spectroscopy
Forensic
Chemometrics
Data fusion

ABSTRACT

Time elapsed since bloodstain deposition is a crucial aspect in forensic investigations, where non-destructive spectroscopic methods play a pivotal role. While extensive research has been conducted by UV–Vis spectroscopy, showcasing its utility in specific cases, there is still a paucity of studies based on NIR spectroscopy, which has the potential to overcome the limitations of the UV–Vis-based methods. To compensate for this disequilibrium, the present study aimed to evaluate the NIR applicability for estimating the age of forensic bloodstains and develop a performance comparison with UV–Vis spectroscopy methods. Capillary blood was sampled and subjected to a 16-day aging, during which it was repeatedly analyzed using both spectroscopic methods. Subsequently, chemometric analysis was applied to process the spectral data and independently assess the methods' performance. Classical preprocessing transforms (i.e., Savitzky-Golay derivatives and SNV transform) were used together with more targeted strategies, such as class centering, whose benefit was highlighted by PCA. Lastly, PLS regression models were computed to evaluate the effectiveness of both spectroscopic methods in estimating the time elapsed since blood trace deposition. Comparable root mean square errors in prediction (RMSEP) – 40 and 55 h for UV–Vis and NIR spectroscopy, respectively – were observed for both techniques, featuring an improvement with respect to the existing literature for NIR spectroscopy. Data fusion strategies for a multi-instrumental platform were also explored, evaluating advantages and disadvantages of low-level and mid-level approaches. The results indicated that NIR spectroscopy integrated with adequate chemometric strategies deserves increased appreciation in forensic bloodstain dating.

1. Introduction

The primary task of forensic sciences is to assist decision-makers in understanding the details of a criminal event and subsequently making informed decisions based on the evaluation of evidence. However, the mere observation of forensic traces is generally not sufficient to qualify their relevance. The crucial role of forensic practitioners is to assign the appropriate significance to these pieces of evidence through their decoding and understanding using specialized knowledge [1], and to communicate these results comprehensibly to non-scientists (such as judges or attorneys) [2]. When the traces are bloodstains, analogous conditions apply. To fully recognize the meaning of blood discovered at the crime scene and/or on objects involved in the incident and adequately estimate the value of the findings, it is necessary to verify whether these traces are related to the considered act of violence. The simple revelation of bloodstains and even their association with a specific individual through genetic analysis may be insufficient to prove their connection with the crime, since the circumstances under which these traces were formed – and precisely the time of their creation – are often questioned. Hence, confirming whether these traces originated during the crime often becomes essential. This information can be provided in a specific way: by answering the question about the time

** Corresponding author.
* Corresponding author.
E-mail addresses: cristina.malegori@unige.it (C. Malegori), paolo.oliveri@unige.it (P. Oliveri).

https://doi.org/10.1016/j.talanta.2024.126444
Received 12 March 2024; Received in revised form 21 May 2024; Accepted 16 June 2024
Available online 18 June 2024

elapsed since bloodstains deposition (TSD).

The issue of bloodstains' age is nothing new for researchers and – most importantly – practitioners in forensic science. It is enough to mention that the initial endeavors to establish the TSD date back to the early 20th century [3]. Comprehensive reviews, including those by Bremmer et al. [4] and Zadora and Menżyk [5], extensively delved into the bloodstains aging process and the techniques developed to ascertain their TSD; hence, they should serve as fundamental sources of information on this matter. Early methods to establish the timing of bloodstain deposition relied on visually comparing changes in blood color [3,6]. However, these procedures were soon supplanted by more sophisticated and objective analytical techniques, including spectrophotometric [7,8], chromatographic [9,10] or spectroscopic approaches [11–14]. In a relatively short time, the methods based on vibrational spectroscopy in the near-infrared (NIR) [11,15,16] and Raman spectroscopy [13,17–19], along with ultraviolet–visible (UV–Vis) spectroscopy [8,20–24], were primarily used in the blood dating attempts. In fact, after evaporation of the aqueous plasma component, blood degradation mainly involves the iron-containing protein – hemoglobin – present in red blood cells, and the time-dependent transformations of this tetrameric protein are well-reflected in both Raman and UV–Vis spectra, showing characteristic changes during the formation of methemoglobin or hemo- and hemichromes [25]. At the same time, NIR spectroscopy proved effective in observing the progressing dehydration of bloodstain residues and methemoglobin formation at a later aging stage [26]. Considering the complementarity of information provided by different spectroscopic techniques, combining two analytical methods focused on different aspects of blood degradation may contribute to a more accurate estimation of the trace age, even though no studies have been tried so far to implement such a dualistic approach.

Despite various attempts, no method has been universally adopted by the forensic community in consideration of the blood degradation process complexity. The prolonged deadlock may be partly explained by the fact that most proposed solutions were presented through purely scientific/analytical viewpoints rather than through the forensic science lens. In other words, the blood dating models were developed to provide a universal chronological solution, overlooking the fact that forensic science is not merely extrapolative (i.e., the result can be predicted by setting up reproducible experiments and developing a regression model), but rather retrodictive and contextual. In the case of bloodstain dating, the context primarily consists of the environmental conditions at the crime scene, which render the particular case somewhat unique. These conditions are highly significant in determining the course and rate of blood degradation processes and thus influence the sought-after answer, i.e., the bloodstain age.

In recent years, an alternative approach to address the blood dating challenge has been suggested [27–29]. This proposal implies that the variability in aging kinetics may be mitigated by replacing the conventional dating methodology with a case-specific comparative analysis. The fundamental concept involves assessing the (dis)similarity between the stage of evidence decomposition and sets of reference materials, namely bloodstains experiencing simultaneous aging under the degradation conditions found at the crime scene or recreating them as accurately as possible. However, the development of a standardized procedure is still required.

In order to provide such a method, the present study combines two spectroscopic techniques – UV–Vis and NIR – to better understand the transformations occurring during bloodstain aging. In particular, the ability to monitor the blood degradation processes and to predict the bloodstains age was considered using both individual methods and their combination. To make this comparison, partial least squares (PLS) regression was used to build age-predicting models from spectral data, while their performance was expressed by the root mean square error of prediction (RMSEP). Lastly, data fusion of the NIR and UV–Vis spectroscopic data led to a combined PLS model.

Given the possible difficulty of employing different analytical methods in real-case scenarios, some general practical suggestions for forensic dating are proposed in the Document S1 of Supplementary Material. Those suggestions are intended to give an input to standardize the entire procedure, particularly for forensic technicians, regarding the measures for securing and storing traces intended for dating purposes.

2. Materials and methods

2.1. Sampling

Blood samples were obtained from five healthy volunteers, three males and two females, aged between 25 and 41 years (average = 31). Blood was drawn directly from the fingertip by finger-puncturing, then it was recovered with a quantitative pipette and deposited for analysis without the addition of any anticoagulant agent. For each donor, the blood deposition was done at least in triplicate to account for variability.

For UV–Vis analysis, 20 μl aliquots of blood were deposited onto glass slides (Pearl Microscope Slides – 1.0–1.2 mm thickness) and immediately smeared to obtain a thin layer of blood. For NIR analysis, 20 μl aliquots of blood were deposited directly onto the inner flat face of optical glass cells (Precision Cell, Hellma Analytics, Milan, Italy) and left to dry. Sample preparation is visually summarised in Fig. S1.A in Supplementary Material.

2.2. Aging conditions

After deposition, all samples were left to dry in the dark at controlled laboratory conditions (T = 20 ± 2 °C, humidity = 41 ± 2 %). Samples were deposited on day 0 (Monday) and analyzed with both UV–Vis and NIR spectroscopies every 24 h (at the same hour) during working days starting from day 1, as reported in Figure S1.B in Supplementary Material. Samples were monitored for 16 days, with a total of 12 samplings.

The same analytical procedure was repeated in four sessions: December 2022 (Winter session), March 2023 (Spring session), June 2023 (Summer session 1), and July 2023 (Summer session 2). Not all subjects provided blood in all sessions, as is detailed in Table 1. Each subject provided three bloodstains per technique for each session, except subject S, who provided six samples for each technique in the winter session (marked by * in Table 1). In total, 27 bloodstains were analyzed with each technique throughout the whole duration of the study.

2.3. Instrumentation

UV–Vis analysis was performed with a Cary-100 UV–Vis Spectrophotometer (Agilent Technologies – Santa Clara, CA, USA) equipped with a horizontal sampling integrating sphere working in diffuse reflection mode. The range of spectral acquisition was 350–900 nm, with a resolution of 1.0 nm. The averaging time was 0.1 s, with a data interval of 1.0 nm and a scan rate of 600 nm/min. The spectral bandwidth was 4.0 nm. The glass support was fixed vertically on a sample holder, ensuring that the layer of blood covered the whole window as homogeneously as possible. Additionally, a disk made of Spectralon® was placed behind the glass substrate, serving as a highly reflective material, to maximize the amount of radiation reaching the integrating sphere and the detector, through transflection. Sample position on the holder was maintained day by day. Three consecutive replicates were

Table 1
Sampling scheme according to blood donor per session.

	Subject				
Session	"S"	"R"	"P"	"C"	"O"
Winter	✔*				
Spring	✔	✔			
Summer 1	✔	✔	✔		
Summer 2				✔	✔

taken at every sampling time, with a total of 972 spectra collected in the UV–Vis spectral range (27 bloodstains × 3 repetitions × 12 days of analysis).

NIR analyses were performed using a NIRFlex Solids FT-NIR spectrophotometer, BUCHI (BUCHI s.r.l, Flawil, Switzerland), operating in transflection mode. To obtain transflection, the bloodstain was covered by a transflector, an accessory in 360L steel with a fixed path length. The range of spectral acquisition was 4000–10,000 cm^{-1}, with a data interval of 4.0 cm^{-1} and a number of scans per measurement equal to 32. A window reducer of 3 mm diameter was applied for the analysis to ensure that the analyzed sample completely covered the measuring window. Samples were analyzed in triplicate each day, slightly moving the sample between replicates, with a total of 972 spectra (27 bloodstains × 3 repetitions × 12 days of analysis) collected in the NIR spectral range.

2.4. Data analysis

2.4.1. Data organization

Spectral data were organized into data matrices using MATLAB® version 2023a (MathWorks, Natick, MA, USA). UV–Vis and NIR data were organized in two independent matrices with samples on the rows (972 rows) and variables on the columns, with 551 wavelengths for UV–Vis data and 1501 wavenumbers for NIR data. Then, the mean spectrum for each sample on a specific day was calculated from the three replicates. The dimensions of the resulting matrices were 324 × 551 and 324 × 1501 respectively. The data matrices underwent multivariate data analysis [30] with PLS_Toolbox 9.2 (Eigenvector Research Inc., Manson, WA, USA) under the MATLAB® environment.

2.4.2. Data exploration

NIR spectra were converted from reflectance to the pseudo-absorbance scale (log (1/R)) to improve their interpretability [31]. Exploratory data analysis was performed by principal component analysis (PCA) [32], initially on the raw data, in order to verify the dependence of sample distribution on different factors, namely subject, analytical session, single bloodstain and time.

Data were preprocessed to remove the sources of variation non-pertaining to the effect of time from deposition. Classical line preprocessing techniques were tested, i.e., standard normal variate (SNV) transform [33], 1st and 2nd derivative with Savitzky-Golay algorithm [34], together with a groupwise column scaling known as class-centering, whose mathematical expression is detailed in Eq. (1):

$$\lambda_{BS\ t_i\ cc} = \lambda_{BS\ t_i} - \frac{\sum_{i=1}^{n} \lambda_{BS\ t_i}}{n} \quad (1)$$

where $\lambda_{BS\ t_i\ cc}$ is the class-centered absorbance value at wavelength λ, for sample BS at time i, $\lambda_{BS\ t_i}$ is the absorbance value at wavelength λ for sample BS at time i, and n is the total number of sampling points [35].

PCA was then repeated on the preprocessed data.

2.4.3. Multivariate regression

Partial least squares (PLS) regression models were calculated from the two data matrices, using the time since blood deposition as the response variable (Y) [36,37]. To build the regression model, data were divided into a training and a test set. The training set comprised a total of 216 spectra, corresponding to data collected during the first three analytical sessions ("Winter session", "Spring session", and "Summer session 1" – see Table 1). These sessions involved 18 bloodstains from three out of five subjects ("S", "P", and "R"), encompassing one female and two males, and spanned over 12 sampling times. The test set, consisting of the remaining 72 spectra from "Summer session 2", was intentionally chosen to be entirely independent from the training set. In fact, this set consisted of six bloodstains from two different subjects ("C" and "O") not included in the training set.

Several PLS models were built from the training set and compared to optimize the data preprocessing using the model optimizer option of the PLS_Toolbox. The following row preprocessing transforms were considered.

- 1st derivative, Savitzky-Golay algorithm with 11-point window size and 2nd-degree interpolating function [34];
- 2nd derivative, Savitzky-Golay algorithm with 11-point window size and 2nd-degree interpolating function [34];
- SNV [33];
- Normalization obtained by division of each variable by the sum of the absolute value of all selected variables for the given sample, returning a vector with the area under the curve equal to 1 [38] (referred to in the text as Norm1);
- Normalization obtained by taking the square root of the sum of the squared values of all selected variables for the given sample, returning a vector of length equal to 1 [38] (referred to in the text as Norm2).

These transforms were employed individually or in combination with one another (multi-stage preprocessing). Some of the tested strategies involved an additional step of class-centering (Eq. (1)), implemented before column mean centering of the data matrix (applied each time). Additionally, model construction without any preprocessing, apart from column mean centering, was also explored. The combination of the described options eventually led to the construction of 92 models for each technique.

For cross-validation [39], a block scheme was applied, in which spectra corresponding to one bloodstain at all sampling times were excluded from model construction at each cross-validation cycle, and the excluded bloodstain was then used for prediction. The root mean square error in cross-validation (RMSECV) was calculated and this process was repeated for all bloodstains. A mean RMSECV was then computed and presented as the final RMSECV for that particular model. This cross-validation technique is referred to in the text as sample-wise cross-validation and it was applied to have a cross-validation set as independent as possible from the training set, for model optimization purposes (i.e., for the choice of the optimal complexity in terms of number of latent variables). Indeed, this technique ensures that each sampling time of each specific sample is predicted on a model built on different samples, thus reducing the possibility of overestimating the performances of the model. The best model for prediction was selected by minimizing the RMSECV and opting for the model with the fewest latent variables.

A permutation test was employed on the selected models to assess their comprehensive reliability, using the built-in tool in the PLS_Toolbox 9.2 [40]. The permutation test randomizes the order of rows in the data matrix X while keeping the response vector Y unchanged. This is done to ascertain whether the chosen model performance significantly differs from the one of a random model constructed using the same data after breaking the correlation patterns [41].

The final models were subsequently applied to the test set to evaluate the regression predictive capability. The root mean square error in prediction (RMSEP) was calculated from the test set data as an indicator of the model dating accuracy.

2.4.4. Data fusion

Data fusion was initially conducted through low-level datasets integration [42] consisting in concatenation of variables through matrices juxtaposition. In the present study, different bloodstains were analyzed with UV–Vis and NIR spectroscopy; therefore, a strategy was needed to attribute the data obtained from the two techniques to the same sample. In practice, the information for a specific subject at a specific time was considered as a unique sample. For instance, a mean spectrum was calculated for subject "S" in "Summer Session 1" on the three different bloodstains (S1, S2, S3) at each time, obtaining a unique spectrum for

each subject at each time on the specific technique (Fig. S2 in the Supplementary Material). The unique spectra were then concatenated, juxtaposing UV–Vis and NIR wavelengths in the final matrix, with a number of rows one third of the starting matrix (n) and a number of columns resulting from the sum of the of UV–Vis (p) and NIR (q) variables. Namely, $n/3 = 108$ and $p + q = 551 + 1501 = 2052$.

After concatenating the variables, a new PLS model on the fused data was calculated. Preprocessing on the fused variables was applied with two different approaches.

1. Fusion of data preprocessed according to the method chosen after the optimization described in Section 2.4.3. In this way, optimization of the preprocessing procedure for NIR and UV–Vis data is conducted independently and then one model is calculated on the fused data.
2. Fusion of raw data from NIR and UV–Vis and subsequent preprocessing on the fused matrix using the optimization process described in Section 2.4.3. In this way, NIR and UV–Vis spectra are preprocessed in the same way, with the potential advantage that the optimization represents the final step after completing the data fusion.

Low-level data fusion regression models were calculated after application of the two preprocessing strategies and the ultimate model was selected by minimizing RMSECV and computed through sample-wise cross-validation. The model performance was further assessed using a permutation test. The training and test set division followed the same strategy described for the non-fused matrices, resulting in 72 rows (6 samples × 12 times) in the training set and 24 rows (2 samples × 12 times) in the test set. The final step in low-level data fusion applied the model to the test set and calculated the RMSEP.

As last step, mid-level data fusion was applied by combining the significant latent variables obtained from independent regression models built with data from the two techniques applied on the same samples [43]. To achieve this, the samples analyzed by the two spectroscopies had to be made comparable. Therefore, the same strategy described for low-level data fusion was applied, concatenating a single subject in a single session as the same sample. After concatenating the significant latent variables, samples were again divided into training and test sets, following the procedure described for low-level data fusion. A new PLS model was then constructed on the new variables, using sample-wise cross-validation for model selection (optimization step) and a permutation test for model evaluation. Lastly, the model was applied to the test set data, and RMSEP was calculated for validation purposes.

The significance of the differences in performances used to compare both single-instrument and fused regression models was calculated using a Fisher's F test between squared RMSEP, with degrees of freedom corresponding to the number of samples in the test set. A difference was considered significative when $p < 0.1$, i.e. probability > 90 %, and slightly significant when $p < 0.2$, i.e. probability > 80 %.

3. Results and discussion

3.1. Comparison between UV–Vis and NIR

3.1.1. Chemical interpretation of changes during aging

Raw and averaged UV–Vis and NIR spectra are reported in Fig. 1. The raw UV–Vis spectra (Fig. 1.A) include the individual spectra from all analyzed bloodstains, recorded at every time and color-coded based on

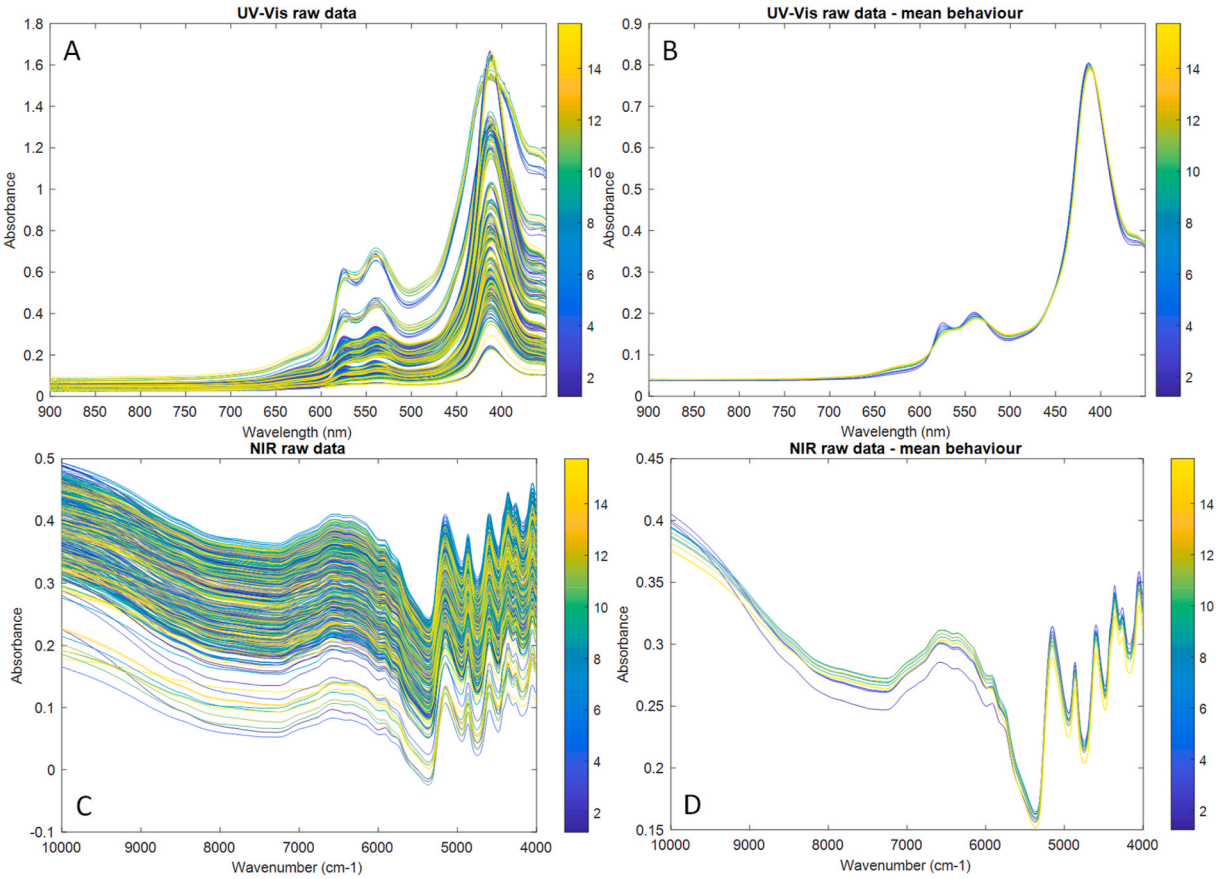

Fig. 1. A: UV–Vis raw data; B: Average behavior of UV–Vis data, obtained by operating a mean of all samples for each specific time; C: NIR raw data; D: average behavior of NIR data, obtained by operating a mean of all samples for each specific time. All graphs are colored according to time, going from day 1 (dark blue) to day 16 (light yellow).

the time elapsed since deposition. The corresponding averaged spectra, each representing all signals recorded at a given time and coded with a distinct color, are shown in Fig. 1.B. Time-dependent changes are readily observed in UV–Vis spectra even by visual inspection, especially in the 350–700 nm range. Notably, the Soret band's maximum – initially at ca. 420 nm – changed with sample degradation, showing a so-called blue shift, i.e., a shift of the maximum towards lower wavelengths [25]. This change is accompanied by various distortions in the 500–650 nm region, which encompasses, among others, the so-called Q-bands [8] which are classified further into alpha (α) and beta (β) bands. In fresh bloodstains dominated by oxyhemoglobin, the corresponding maxima are located at 542 and 576 nm respectively, whose time-dependent evolution involves attenuation, broadening, and merging into a single band, all changes indicating methemoglobin formation with increasing TSD. The oxyhemoglobin conversion to methemoglobin was also denoted by a gradual absorbance increase at an approximate wavelength of 630 nm [44]. All the above observations are consistent with previous literature reports [8,12,20–22,24]. Both Q-band and Soret band were interpreted as π/π^* transitions, arising from the electron delocalization extending across the tetrapyrrole ring of porphyrins [45]. Since these bands exhibit high sensitivity to structural alterations, particularly during ligand exchange processes occurring through the nitrogen atoms of pyrrole rings, their distortions resulting from new hemoglobin derivatives formation are readily justified.

The raw NIR spectra reported in Fig. 1.C depict the spectral features corresponding to all analyzed bloodstains, while Fig. 1.D presents the averaged color-coded signals based on the time elapsed since deposition. The visual inspection of the averaged spectra reveals that certain spectral changes are evident. However, their interpretation is considerably more challenging than that of UV–Vis spectra, especially without the preliminary signal processing stage. Notably, an intensity decrease with TSD is evident in the range of 10,000–9500 cm^{-1}, in combination with the occurrence of an isosbestic point around 9500 cm^{-1}. In the initial stages of degradation (approximately the first six days after the traces are formed), a significant change in absorption between 8000 and 6500 cm^{-1} (the O–H stretching first overtone vibration region) is observed. These variations weaken in a more advanced stage of degradation – as evidenced by the preprocessing in Fig. 1.D. Observed spectral alterations can be explained by the expected rapid process of water evaporation in the first days and then a stabilization of the process. The reduced variability in this region during the following days can be partly attributed to scattering effects and spectral distortions due to path length variations of electromagnetic radiation stemming from alterations in measurement geometry, sample thickness or its physical properties [46]. Another explanation for the minimal spectral changes is the occurrence of bands corresponding to proteins (hemoglobin, albumin, globulin) in the 6000–5700 cm^{-1} range, more precisely related to the first overtone of –CH stretching vibrations [26].

Around 5200 cm^{-1} a maximum in the water band is expected, resulting from the combination of O–H stretching, O–H deformation and O–H bending second overtone. Accordingly, its intensity decreases with TSD due to water loss. Compared to the first O–H stretching overtone, the stronger correlation of this combination band with aging may stem from its higher intensity in the NIR spectrum. Indeed, this spectral region was successfully used by Botonjic-Sehic et al. [11] to estimate the TSD. Finally, protein absorption bands are found in the 5000–4000 cm^{-1} range, including (i) N–H bending second overtone, (ii) the combination of C–H stretching and C═O stretching, (iii) the combination of C–O stretching, N–H in-plane bending and C–N stretching [47]. Their decreasing intensity with bloodstains aging can be explained by the degradation of protein structures, namely hemoglobin, albumin, and/or globulin [26].

3.1.2. Unsupervised analysis

The score plots of PCA elaborated from raw data of both UV–Vis spectroscopy and NIR spectroscopy are showed in Fig. 2, respectively in section A and B. For both techniques, score plots have been colored according to sample (A.1/B.1), time (A.2/B.2), session (A.3/B.3) and subject (A.4/B.4). From a first observation, UV–Vis plots are characterized by strong grouping according to sample, meaning that the differences between the spectra of the various bloodstains are the main source of variability. It is noteworthy that this variability dominates over potential subject-dependent and session-dependent sources of variability. In fact, two bloodstains from the same subject in the same analytical session (for instance, R1 and R2 in Fig. 2.A.1) are located further apart on the score space than two bloodstains from different subjects in different analytical sessions (for instance, P4 and R2 in the same figure). No other trend is noticeable in the PC space. Indeed, no clear time trend is evident in Fig. 2.A.2 and no significant grouping can be observed in Fig. 2.A.3 and Fig. 2.A.4.

On the contrary, virtually no grouping according to sample can be observed on the score plots obtained from NIR data (Fig. 2.B.1). Very limited group separation is observed resulting from time evolution (Fig. 2.B.2), even though a hint of trend along PC2 can be seen. When the score space is colored according to the analytical session (Fig. 2.B.3), some hint of grouping can be drawn, even if all the groups are partly overlapping. The same trend is observed about the effect of the subject grouping (Fig. 2.B.4).

In order to correct the sample-related variability observed in UV–Vis spectra, a specific preprocessing (class-centering) was applied after the SNV transform on UV–Vis data. Only SNV transform was applied to NIR data. Then, PCA was repeated on preprocessed data and the results are displayed in Fig. 3. The comparison between Fig. 2.A.1 and Fig. 3.A.1 reveals that the pretreatment efficiently removed the predominant effect of sample variability for UV–Vis spectroscopy. Upon this removal, the chronological evolution of bloodspots can be recognized as the primary source of data variability (Fig. 3.A.2). In particular, the progressive blood degradation is recorded by a shift of the PC1 score values from positive to negative. No clusters can be detected in Fig. 3A.3 and Fig. 3. A.4, confirming that the specific analytical session and blood donor did not introduce a bias in the spectral dataset.

Preprocessing proved beneficial in evidencing the chronological evolution of bloodspots (Fig. 3.B.2) for NIR spectra as well, as is evident in a simultaneous shift of PC1 and PC2 scores along an oblique direction. A slight grouping according to samples, analytical session and subject is still evident in Fig. 3.B.1, 3.B.3, and 3.B.4, which was not improved nor worsened by the preprocessing.

From the loading distribution on PC1, in the PCA for preprocessed UV–Vis data (Fig. 4.A), negative contributions from the methemoglobin band and the Soret band (at higher wavenumbers) are evident. Positive contributions from Q-bands and the Soret band (at lower wavenumbers) are also observed. A comprehensive interpretation of scores and loadings reveals that higher absorbances in the methemoglobin band and higher wavenumbers in the maximum of the Soret band are characteristic of aged samples. Conversely, higher absorbances in the Q-bands and lower wavenumbers in the maximum of the Soret band are typical for newly deposited samples, as already noted from visual inspection. The band attribution, explained on preprocessed data for clarity, is also deducible from raw data [15].

From the loading distribution in the PCA on NIR data (Fig. 4.B), it can be deduced that PC1 mainly concerns the region of the protein bands. In particular, higher values of PC1 represent samples with higher intensities in the protein bands. A joint interpretation with the score plot reveals that this area of the orthogonal space corresponds to newly deposited bloodstains. Accordingly, the aged samples show negative PC1 values. PC2 loadings overweight the water stretching and bending combination band, for which higher intensities result in higher PC2 scores. The same is observed for a band around 6300 cm^{-1} attributed to the C–H group of amide bonds. The combined interpretation of score and loading plots reveals that newly deposited samples are characterized by higher PC2 scores, confirming that these samples contain a higher amount of water (higher intensities in the water absorption band).

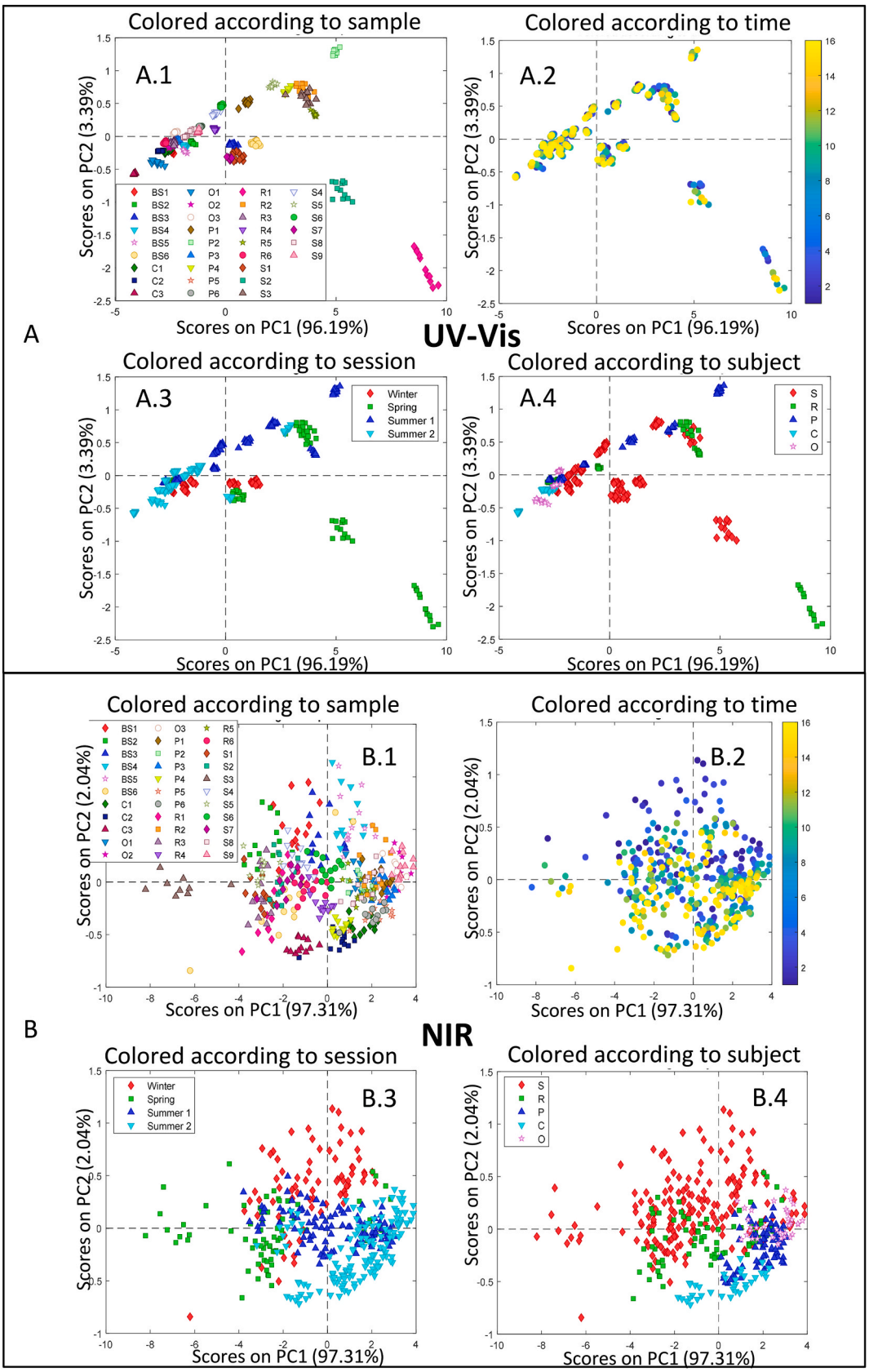

Fig. 2. PC score plots for raw data. A: Score plot from UV–Vis spectra. A.1: Score plot colored according to single bloodstain; A.2: Score plot colored according to time; A.3: Score plot colored according to analytical session; A.4: Score plot colored according to different subject. B: Score plot from NIR spectra. B.1: Score plot colored according to single bloodstain; B.2: Score plot colored according to time; B.3: Score plot colored according to analytical session; B.4: Score plot colored according to different subject.

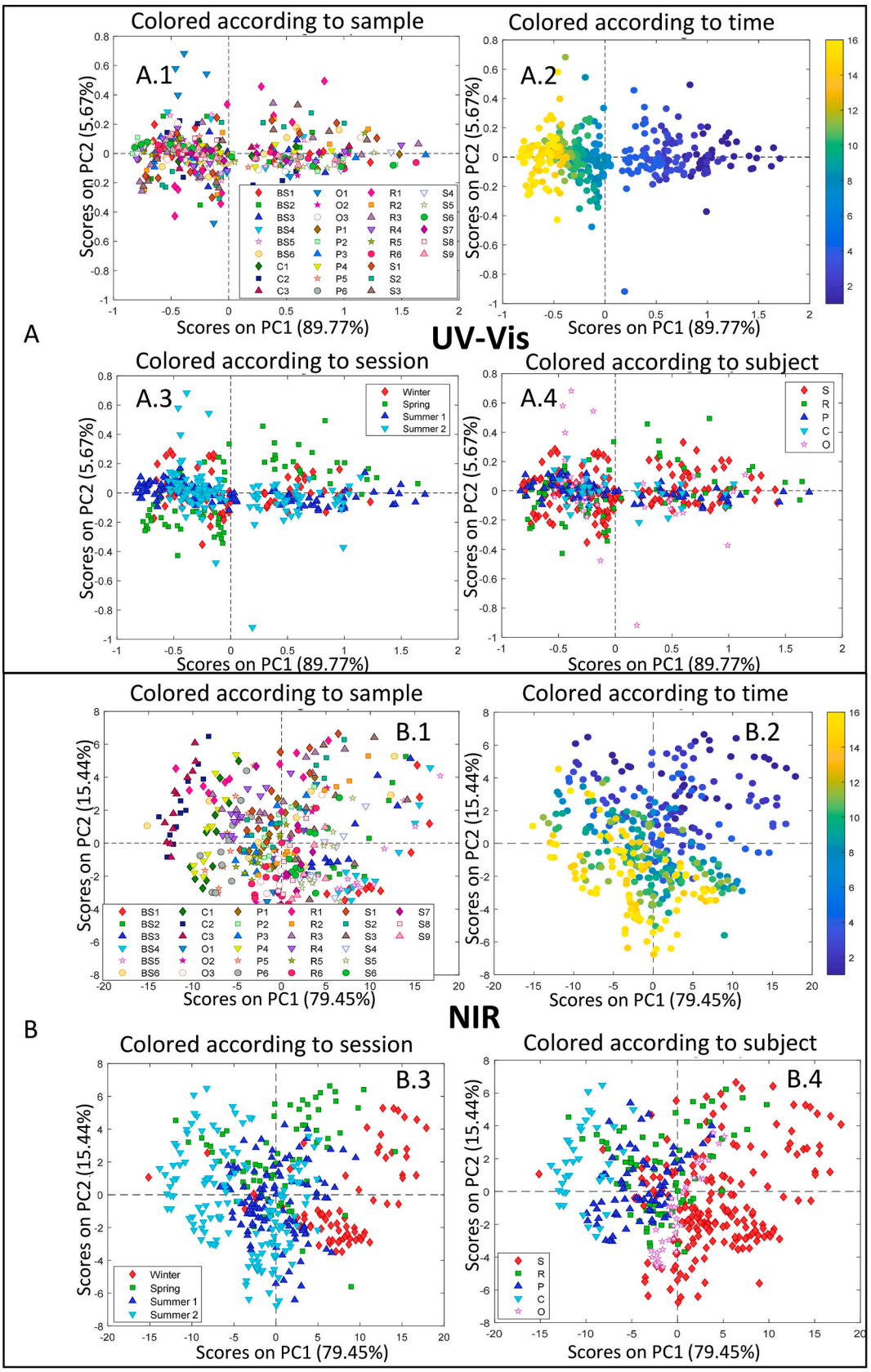

Fig. 3. PC score plots for preprocessed data. A: Score plot from UV–Vis spectra. Preprocessing = SNV + class centering. A.1: Score plot colored according to single bloodstain; A.2: Score plot colored according to time; A.3: Score plot colored according to analytical session; A.4: Score plot colored according to different subject. B: Score plot from NIR spectra. Preprocessing = 1st derivative + SNV. B.1: Score plot colored according to single bloodstain; B.2: Score plot colored according to time; B.3: Score plot colored according to analytical session; B.4: Score plot colored according to different subject.

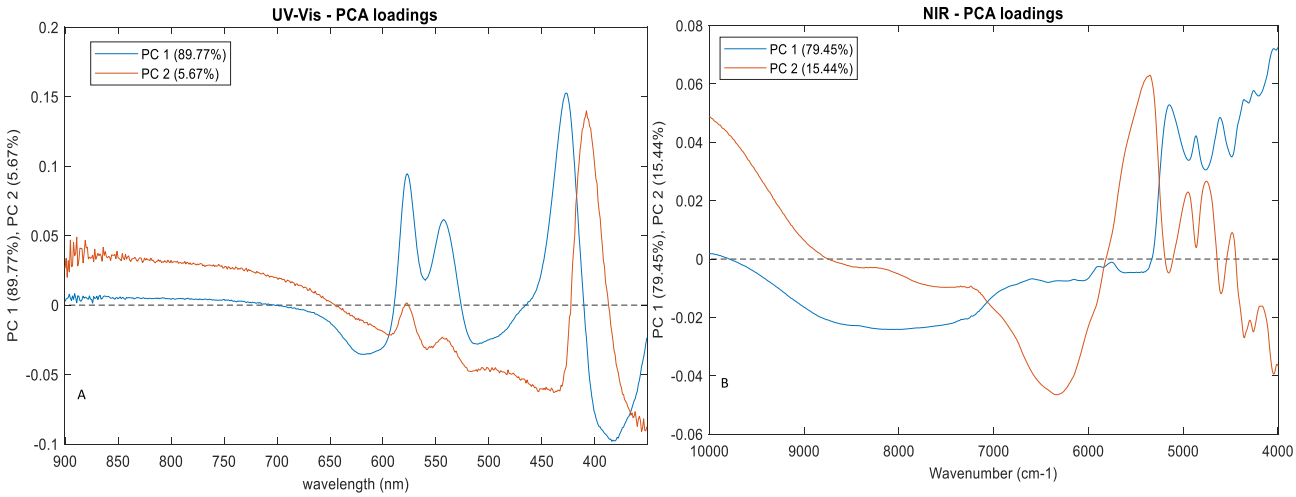

Fig. 4. A: Loadings of PC1 and PC2 (preprocessing = SNV transform + class-centering) for PCA performed on UV–Vis spectra; B: Loadings of PC1 and PC2 (preprocessing = SNV transform) for the PCA performed on NIR spectra.

3.1.3. *Supervised analysis*

After completing the data exploration, regression models were optimized to predict the bloodstains' TSD. Out of the 92 tested combinations of preprocessing protocols preceding the model computation, the one offering the best output for UV–Vis data was the one implying the first derivative followed by normalization (Norm1) and class centering. The selection was made according to the smallest RMSECV (0.97 days) and low number of latent variables (LVs = 5). It was also noted that, among the 92 preprocessing combinations, all 46 containing class centering produced better performances than the 46 not involving class centering. The best model not involving class centering was normalization (Norm1), followed by the first derivative for UV–Vis data (RMSECV = 1.67, LVs = 9). For NIR data, the best preprocessing technique was first derivative, followed by SNV transform (RMSECV = 2.20, LVs = 5). No model containing class centering was rated among the 20 best options. Details on some of the best-performing models are reported in Table 2. The three best models underwent a permutation test. All proved significantly ($p < 0.005$) better than models built on data with broken correlation structure.

The three models were validated with the test set, verifying their prediction accuracy in assessing the bloodstain age. The results, represented also graphically in Fig. 5, show that the class-centered UV–Vis model provides the best accuracy for bloodstain dating, with RMSEP = 1.67 days, *i.e.*, about 40 h. On the contrary, when class-centering is not applied, UV–Vis spectroscopy gives an error of 3.18 days, around 76 h. The best NIR model yielded an RMSEP of 2.30 days, corresponding to 55 h. R^2 was always above 0.8, while the prediction bias does not highlight any systematic deviation of the model being in most of the cases lower than 1. It is worthily noticeable that a higher bias is present in the UV–Vis models in particular when class-centering is not performed; this could indicate that the systematic effect, when present, is due to differences in subjects, properly corrected by signal preprocessing. Conversely, these considerations are not applicable to NIR models where bias can be considered not relevant.

3.2. Data fusion

Upon NIR and UV–Vis spectroscopy data fusion, the model optimization process was repeated. Both low- and mid-level data fusion models were built with two approaches, namely using or avoiding class-centering. Again, the best model was selected according to RMSECV, calculated by sample-wise cross-validation.

The results for the first low-level data fusion model are shown in Fig. S.3.A (Supplementary Material), which yielded a RMSEP of 1.62 days, corresponding to about 39 h. The second approach, implying raw data fusion before preprocessing and testing 46 preprocessing combinations without class-centering, produced the best results when the first derivative was followed by normalization (Norm1). Application of this method to the test set provided a RMSEP of 2.82 days, corresponding to about 68 h, as shown in Fig. S.3.B. R^2 was always over 0.85, while prediction bias was low (0.59 days) for the model using class-centering and high (2.07 days) for the model without this preprocessing, confirming the previous observation that bias, when present, is mainly due to the differences among bloodstains.

The results of PLS models built on mid-level data fusion are shown in Fig. 6. Again, two different approaches were used to calculate the models, one including class-centering with ten initial variables (5 LVs from the NIR PLS model and 5 LVs from the UV–Vis PLS model) and one avoiding it, with 14 initial variables (5 LVs from the NIR PLS model and 9 LVs from the UV–Vis PLS model). The number of variables provided by each individual model was decided according to the significant latent variables determined during the supervised analysis. The two new

Table 2
Summary of figures of merit for the selected regression models.

Data	Preprocessing	Latent Variables	RMSEC (days)	RMSECV (days)	RMSEP (days)	R^2	Prediction bias
UV–Vis	1st derivative + Norm1 + class-centering	5	0.74	0.96	1.67	0.96	0.37
UV–Vis	Norm1 + 1st derivative	9	1.18	1.67	3.18	0.88	1.14
NIR	1st derivative + SNV	5	2.03	2.20	2.30	0.83	0.88
Low-level data fusion	UV–Vis: 1st derivative + Norm1 + class-centering; NIR: 1st derivative + SNV	5	0.49	0.91	1.62	0.95	0.59
Low-level data fusion	1st derivative + Norm1	5	1.26	1.78	2.82	0.87	2.07
Mid-level data fusion	UV–Vis: 1st derivative + Norm1 + class-centering; NIR: 1st derivative + SNV	5	0.85	1.04	1.48	0.96	0.35
Mid-level data fusion	UV–Vis: Norm1 + 1st derivative; NIR: 1st derivative + SNV	5	1.38	2.14	2.29	0.82	0.87

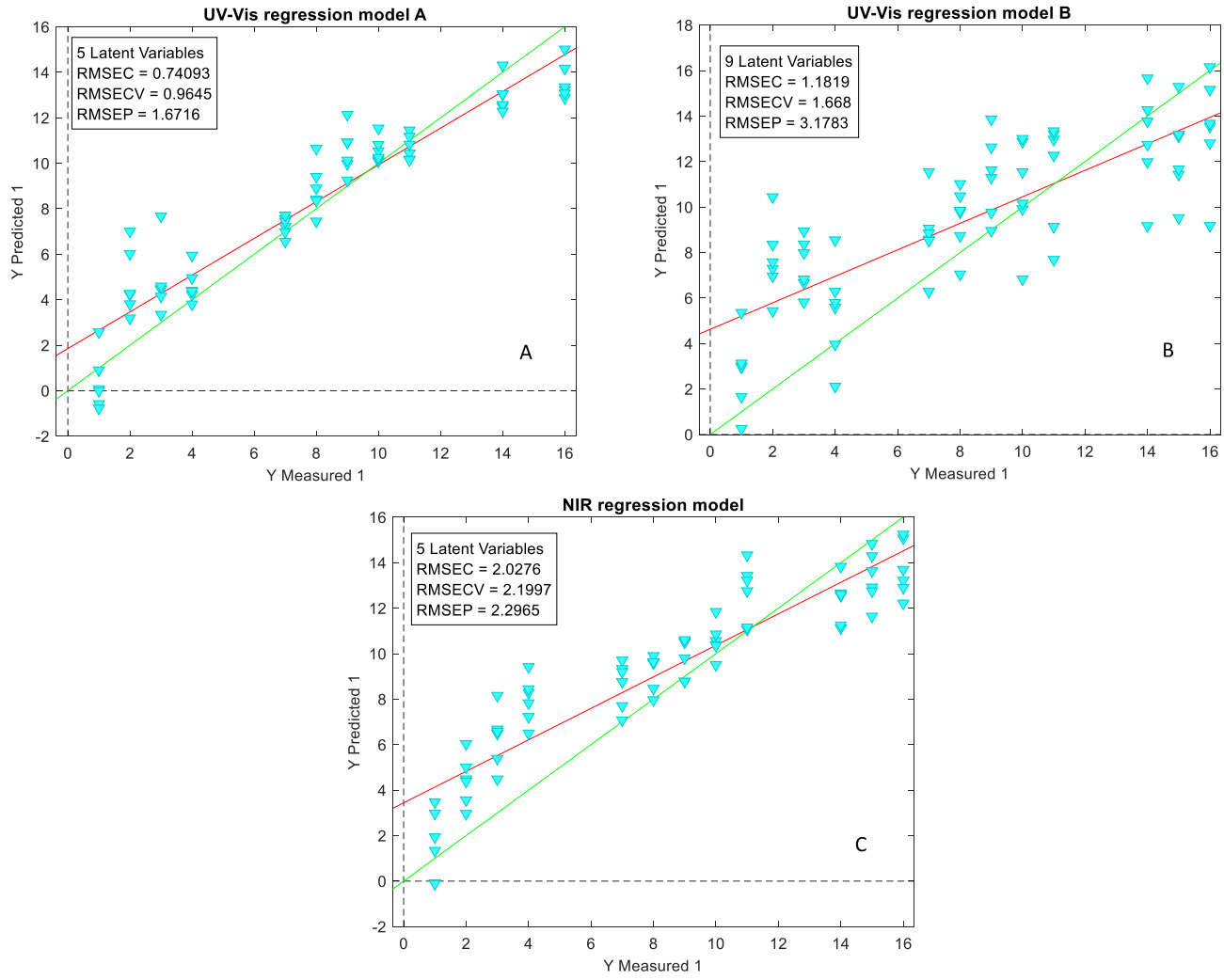

Fig. 5. Results of the application of PLS regression models on the test set. A: Model for UV–Vis data, preprocessing = 1st derivative + Norm1 + class-centering; B: Model for UV–Vis data, preprocessing = Norm1 + 1st derivative; C: Model for NIR data, preprocessing = 1st derivative + SNV.

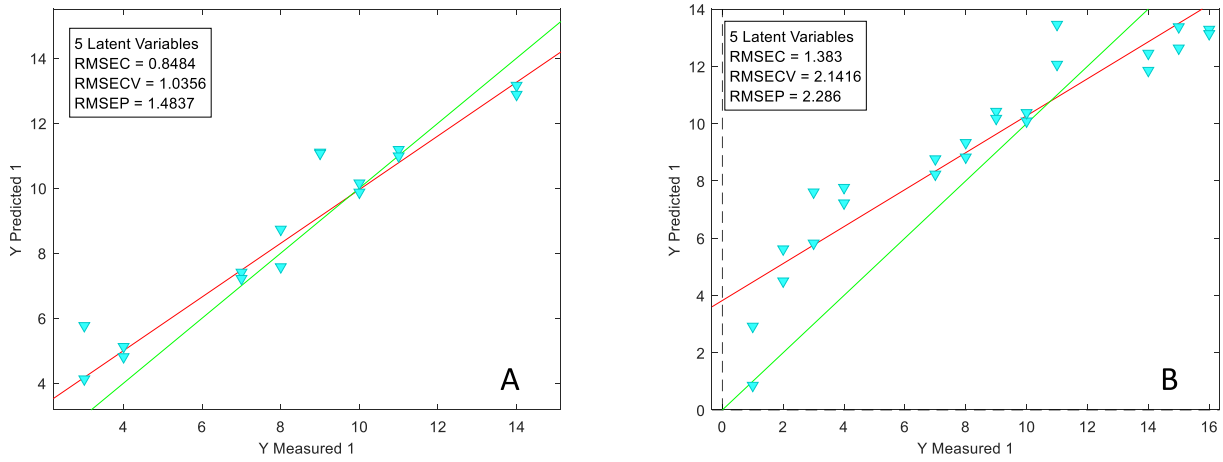

Fig. 6. Results of PLS-R models calculated on mid-level fused data, calculated either with (A) or without (B) the use of class-centering as a preprocessing.

models had five significant latent variables and a RMSEP of 1.48 days (35.5 h, Fig. 6.A) and 2.29 days (about 55 h, Fig. 6.B) respectively. R^2 was always above 0.8 and prediction bias was always lower than 1 day.

3.3. Comparison between UV-VIS and NIR

The initial data exploration reveals that UV–Vis data are more subjected to the effect of sample variability than NIR data. Therefore, UV–Vis data need a "stronger" preprocessing to extract meaningful

information for bloodspot dating.

It should also be noted that the main criticism about the preprocessing adopted is not related to its mathematical calculation, which is relatively easy, but about the strategy itself (Eq. (1)), which requires to complete the chronological series along the investigated period (16 days, in the present case) to be finalized. Indeed, the mean spectrum calculation, which is obtained from averaging all specific spectra along the chronological sequence and subtracting the averaged signal from each spectrum, varies according to the number of sampling times considered and their temporal extension. In theory, the number of sampling points and the time covered should be the same for the training and test set data, which does not represent a problem in a designed setup, but may be impossible in real-case scenarios, where a crime is rarely discovered immediately after its occurrence. In practice, the chronological spectral sequence cannot start from time 0. The consequence of this observation is that the performances of UV–Vis spectroscopy should be critically interpreted according to the specific case found in the forensic practice, which may or, most probably, may not enable the use of the best-performing model.

Another interesting point inferred from the observation of both supervised and unsupervised data analysis is the almost complete independence of results from the blood donors, which is true for both UV–Vis and NIR spectroscopy. Indeed, supervised analysis showed that it is possible to predict the TSD of two subjects using a model built on the blood of three independent subjects. Analogous conclusions can be drawn about the results independence from the analytical session, even though the experiments were conducted under laboratory conditions, with temperature and humidity maintained within a reduced variability range.

The quantitative models resulting from supervised analysis, for both NIR and UV–Vis spectroscopy, provided a reasonable prediction of TSD. The best performance was obtained when class-centering was applied on UV–Vis spectra, yielding a prediction error of about 40 h, which is significantly lower ($p < 0.1$) than that obtained from NIR spectra, around 50 h. The model dating performances observed in the present study are comparable to those reported in the previous literature, calculating a RMSEP for the models developed for NIR data of approximately 2.7 days [26], and RMSEP values oscillating around one day for the UV–Vis models [20,24,48,49]. The situation is reversed when class-centering is not applied: in this case, RMSEP for UV–Vis spectroscopy considerably deteriorates, reaching 76 h, which represents a significantly worse performance ($p < 0.1$) compared to the 55 h resulting from NIR spectroscopy. As commented before, this outcome suggests that in real-case scenarios NIR spectroscopy might be preferable over UV–Vis spectroscopy in terms of performance.

Another interesting observation is that the construction and optimization of the 20 best PLS models built from NIR spectra never implied the use of class-centering, suggesting that there is strong independence of NIR spectra from their preprocessing, a condition that makes the NIR technique more robust than UV–Vis spectroscopy. The robustness of NIR spectroscopy is also confirmed by the fact that the variation between RMSE in construction, cross-validation and prediction is minimal (RMSECV – RMSEC = 0.176 days; RMSEP – RMSEC = −0.103 days; RMSEP – RMSECV = −0.279 days) with respect to UV–Vis spectroscopy both when class-centering is applied (RMSECV – RMSEC = 0.224 days; RMSEP – RMSEC = 0.931; RMSEP – RMSECV = 0.707 days) or not applied (RMSECV – RMSEC = 0.483; RMSEP – RMSEC = 1.993 days; RMSEP – RMSECV = 1.510). Indeed, a low delta between RMSEC, RMSECV and RMSEP usually indicates a lower probability of model overfitting [39].

The significance of the present models was also confirmed by the permutation test, which proved their statistical difference with a 95 % confidence from models built on data with broken correlation structure. This confirms that PLS was able to model structured information correlated to TSD. With reference to the number of latent variables, it is interesting to note that the NIR model and the class-centered UV–Vis model share the same low complexity. In contrast, model complexity increases when class-centering is not applied.

Low-level data fusion did not appear to provide any significant improvement in the TSD estimation, since also in the best-case scenario, namely when class-centering is applied, the resulting RMSEP was about 39 h, a result comparable to what obtained with UV–Vis spectroscopy alone under the same conditions ($p > 0.2$). The low-level data fusion not implying class-centering provided a RMSEP of 68 h, which is higher than the 55 h obtained by NIR alone, even though this difference is only slightly significant ($p < 0.2$). On the other hand, mid-level data fusion led to a RMSEP decrease, reaching 35 h when class-centering was applied. This is the lowest RMSEP value obtained in the present study, indicating that data fusion might improve the dating performances of the models. In this case, this strategy reduced the prevision error of about 5 h with respect to UV–Vis alone, which is an interesting outcome, even though not statistically significant ($p > 0.2$), probably due to the low number of samples. This observation should be confirmed in future studies involving a higher number of subjects. In contrast, the RMSEP of the fused model broadens up to about 55 h when no class-centering was applied, which corresponds to what obtained with NIR spectroscopy alone. In this case, no benefit arose from data fusion. These results suggest that, in most real-case scenarios, where the conditions for applying class-centering are missing, NIR spectroscopy alone is the best choice to provide the most accurate dating. On the other hand, there might be some situations in which the best-performing model for UV–Vis spectroscopy can be calculated and, in this situation, mid-level data fusion is the best option.

4. Conclusions

This study endeavored bloodstains dating for forensic purposes using two complementary spectroscopic tools, namely UV–Vis and NIR spectroscopies. This complementarity arises from the different spectroscopic capabilities in monitoring the degradation processes, UV–Vis primarily tracking the structural changes in hemoglobin, while NIR providing information about water loss from the bloodstain. Consequently, it was possible to identify certain differences between UV–Vis and NIR spectroscopies in the bloodstain dating perspective. Indeed, the present study demonstrated that the combination of these mutually complementing pieces of information may help estimating the bloodstains age with higher accuracy.

NIR spectroscopy's (RMSEP ≈ 55 h) robustness and relative independence from preprocessing steps provides higher resilience in forensic applications and is generally preferrable over UV–Vis spectroscopy in real-case scenarios (RMSEP ≈ 76 h). Noteworthily, bloodspot dating by both UV–Vis and NIR spectroscopies showed a somewhat surprising independence from blood donors. This observation holds promise in the potential use of different blood samples for aging studies and practical blood dating beyond those collected from the individuals who left traces at the crime scene. Of course, a study involving more subjects to better account for their biological variability is needed to draw solid conclusions on this point. However, these results can be regarded as an initial suggestion that blood donors might not be influential in building a model for bloodstain dating.

Additionally, analytical sessions exhibited minimal influence on the correctness of the dating procedure. Although it should be emphasized that this study was conducted within a laboratory setting, minimizing the potential impact of environmental conditions, at least in the case of traces revealed indoors it can be advanced that the influence of external conditions may have minimal impact on dating accuracy.

By merging the spectroscopic data in the context of data fusion, an enhancement in the TSD estimation can be recorded only when class-centering can be applied. In these conditions, mid-level data fusion decreased RMSEP, reaching 35 h, i.e. the lowest value obtained in the present study. This provides a confirmation of our initial hypothesis regarding the potential improvement of blood age estimates through the

application of complementary spectroscopic methods, indicating further research directions. By the way, it must be noted that this improvement refers to conditions that can rarely be obtained in real-case scenarios and therefore, in this situation, NIR spectroscopy alone should be the preferrable technique. Further research is needed to try and reach better control over the conditions influencing the UV–Vis response, which might enable to lessen its dependence on preprocessing and thus improve its performances also in real-case conditions.

Exploring the synergies between different spectroscopic methods and advanced chemometric approaches (e.g., data fusion) could unlock a more comprehensive and accurate bloodstain dating methodology. This multidimensional approach holds promise for refining forensic practices and strengthening the reliability of age estimation in criminal investigations, setting the stage for future endeavors to bridge the gap between laboratory findings and real-world forensic challenges [,13, 27–29,50–52].

CRediT authorship contribution statement

Sara Gariglio: Writing – original draft, Formal analysis, Data curation. **Cristina Malegori:** Writing – review & editing, Project administration, Data curation. **Alicja Menżyk:** Writing – review & editing, Data curation, Conceptualization. **Grzegorz Zadora:** Supervision. **Marco Vincenti:** Writing – review & editing, Conceptualization. **Monica Casale:** Supervision. **Paolo Oliveri:** Supervision, Funding acquisition, Conceptualization.

Declaration of competing interest

The authors declare that they have no known competing financial interests or personal relationships that could have appeared to influence the work reported in this paper.

Data availability

Data will be made available on request.

Acknowledgments

Financial support provided by the Italian Ministry of Universities and Research – MUR (Research Project PRIN 2022 n. 20223WBTH8, CUP: D53D23008950006) is gratefully acknowledged.

Appendix A. Supplementary data

Supplementary data to this article can be found online at https://doi.org/10.1016/j.talanta.2024.126444.

References

[1] C. Roux, R. Bucht, F. Crispino, P. De Forest, C. Lennard, P. Margot, M.D. Miranda, N. NicDaeid, O. Ribaux, A. Ross, S. Willis, The Sydney declaration – Revisiting the essence of forensic science through its fundamental principles, Forensic Sci. Int. 332 (2022), https://doi.org/10.1016/j.forsciint.2022.111182.
[2] G. Sauzier, W. Van Bronswijk, S.W. Lewis, Chemometrics in forensic science: approaches and applications, Analyst 146 (2021), https://doi.org/10.1039/d1an00082a.
[3] L. Tomellini, De l'emploi d'une table chromatique pour les taches de sang (une planche hors texte), Arch. d'Antropologie Criminelle Criminol 4 (1907).
[4] R.H. Bremmer, K.G. De Bruin, M.J.C. Van Gemert, T.G. Van Leeuwen, M.C. G. Aalders, Forensic quest for age determination of bloodstains, Forensic Sci. Int. 216 (2012), https://doi.org/10.1016/j.forsciint.2011.07.027.
[5] G. Zadora, A. Menżyk, In the pursuit of the holy grail of forensic science – spectroscopic studies on the estimation of time since deposition of bloodstains, TrAC, Trends Anal. Chem. 105 (2018), https://doi.org/10.1016/j.trac.2018.04.009.
[6] O. Leers, Die forensische Blutuntersuchung, JAMA, J. Am. Med. Assoc. 55 (1910), https://doi.org/10.1001/jama.1910.04330020055034.
[7] D. Patterson, Use of reflectance measurements in assessing the colour changes of ageing bloodstains, Nature 187 (1960), https://doi.org/10.1038/187688a0.
[8] S.S. Kind, D. Patterson, G.W. Owen, Estimation of the age of dried blood stains by a spectrophotometric method, Forensic Sci. 1 (1972), https://doi.org/10.1016/0300-9432(72)90146-X.
[9] H. Inoue, F. Takabe, M. Iwasa, Y. Maeno, Y. Seko, A new marker for estimation of bloodstain age by high performance liquid chromatography, Forensic Sci. Int. 57 (1992), https://doi.org/10.1016/0379-0738(92)90041-T.
[10] H. Inoue, F. Takabe, M. Iwasa, Y. Maeno, Identification of fetal hemoglobin and simultaneous estimation of bloodstain age by high-performance liquid chromatography, Int. J. Leg. Med. 104 (1991), https://doi.org/10.1007/BF01369715.
[11] E. Botonjic-Sehic, C.W. Brown, M. Lamontagne, Mary Tsaparikos, Forensic Application of Near-Infrared Spectroscopy: Aging of Bloodstains, 2009.
[12] R.H. Bremmer, A. Nadort, T.G. van Leeuwen, M.J.C. van Gemert, M.C.G. Aalders, Age estimation of blood stains by hemoglobin derivative determination using reflectance spectroscopy, Forensic Sci. Int. 206 (2011) 166–171, https://doi.org/10.1016/J.FORSCIINT.2010.07.034.
[13] K.C. Doty, G. McLaughlin, I.K. Lednev, A Raman "spectroscopic clock" for bloodstain age determination: the first week after deposition, Anal. Bioanal. Chem. 408 (2016), https://doi.org/10.1007/s00216-016-9486-z.
[14] H. Lin, Y. Zhang, Q. Wang, B. Li, S. Fan, Z. Wang, Species identification of bloodstains by ATR-FTIR spectroscopy: the effects of bloodstain age and the deposition environment, Int. J. Leg. Med. 132 (2018), https://doi.org/10.1007/s00414-017-1634-2.
[15] C. Connolly, M. Illes, J. Fraser, Affect of impact angle variations on area of origin determination in bloodstain pattern analysis, Forensic Sci. Int. 223 (2012), https://doi.org/10.1016/j.forsciint.2012.09.009.
[16] C. Manis, C. Malegori, E. Alladio, M. Vincenti, P. Garofano, F. Barni, A. Berti, P. Oliveri, Non-destructive age estimation of biological fluid stains: an integrated analytical strategy based on near-infrared hyperspectral imaging and multivariate regression, Talanta 245 (2022) 123472, https://doi.org/10.1016/j.talanta.2022.123472.
[17] A. Menżyk, A. Damin, A. Martyna, E. Alladio, M. Vincenti, G. Martra, G. Zadora, Toward a novel framework for bloodstains dating by Raman spectroscopy: how to avoid sample photodamage and subsampling errors, Talanta 209 (2020), https://doi.org/10.1016/j.talanta.2019.120565.
[18] A. Menżyk, A. Martyna, A. Damin, M. Vincenti, G. Zadora, Breaking with trends in forensic dating: a likelihood ratio-based comparison approach, Forensic Sci. Int. 349 (2023), https://doi.org/10.1016/j.forsciint.2023.111763.
[19] S. Boyd, M.F. Bertino, S.J. Seashols, Raman spectroscopy of blood samples for forensic applications, Forensic Sci. Int. 208 (2011), https://doi.org/10.1016/j.forsciint.2010.11.012.
[20] R. Zhang, P. Wang, J. Chen, Y. Tian, J. Gao, Age estimation of bloodstains based on Raman spectroscopy and chemometrics, Spectrochim. Acta Mol. Biomol. Spectrosc. 290 (2023) 122284, https://doi.org/10.1016/J.SAA.2022.122284.
[21] A. Takamura, D. Watanabe, R. Shimada, T. Ozawa, Comprehensive modeling of bloodstain aging by multivariate Raman spectral resolution with kinetics, Commun. Chem. 2 (2019), https://doi.org/10.1038/s42004-019-0217-1.
[22] B. Li, P. Beveridge, W.T. O'Hare, M. Islam, The age estimation of blood stains up to 30 days old using visible wavelength hyperspectral image analysis and linear discriminant analysis, Sci. Justice 53 (2013) 270–277, https://doi.org/10.1016/J.SCIJUS.2013.04.004.
[23] T. Bergmann, F. Heinke, D. Labudde, Towards substrate-independent age estimation of blood stains based on dimensionality reduction and k-nearest neighbor classification of absorbance spectroscopic data, Forensic Sci. Int. 278 (2017), https://doi.org/10.1016/j.forsciint.2017.05.023.
[24] T. Seki, Y.Y. Hsiao, F. Ishizawa, Y. Sugano, Y. Takahashi, Establishment of a random forest regression model to estimate the age of bloodstains based on temporal colorimetric analysis, Leg. Med. (2023) 102343, https://doi.org/10.1016/J.LEGALMED.2023.102343.
[25] R.H. Bremmer, A. Nadort, T.G. van Leeuwen, M.J.C. van Gemert, M.C.G. Aalders, Age estimation of blood stains by hemoglobin derivative determination using reflectance spectroscopy, Forensic Sci. Int. 206 (2011) 166–171, https://doi.org/10.1016/J.FORSCIINT.2010.07.034.
[26] H. Sun, Y. Dong, P. Zhang, Y. Meng, W. Wen, N. Li, Z. Guo, Accurate age estimation of bloodstains based on visible reflectance spectroscopy and chemometrics methods, IEEE Photon. J. 9 (2017), https://doi.org/10.1109/JPHOT.2017.2651580.
[27] E.K. Hanson, J. Ballantyne, A blue spectral shift of the hemoglobin Soret band correlates with the age (time since deposition) of dried bloodstains, PLoS One 5 (2010) 12830, https://doi.org/10.1371/journal.pone.0012830.
[28] G. Edelman, V. Manti, S.M. Van Ruth, T. Van Leeuwen, M. Aalders, Identification and age estimation of blood stains on colored backgrounds by near infrared spectroscopy, Forensic Sci. Int. 220 (2012) 239–244, https://doi.org/10.1016/J.FORSCIINT.2012.03.009.
[29] A. Menzyk, Toward a spectroscopy - based approach for estimating time elapsed since bloodstains deposition. Development of a Novel Framework for Blood Evidence Evaluation, 2021. PhD.
[30] P. Oliveri, C. Malegori, M. Casale, Chemometrics: multivariate analysis of chemical data, in: Chemical Analysis of Food: Techniques and Applications, second ed., 2020, https://doi.org/10.1016/B978-0-12-813266-1.00002-4.
[31] P. Oliveri, C. Malegori, R. Simonetti, M. Casale, The impact of signal pre-processing on the final interpretation of analytical outcomes – a tutorial, Anal. Chim. Acta 1058 (2019), https://doi.org/10.1016/j.aca.2018.10.055.
[32] S. Wold, K. Esbensen, P. Geladi, Principal component analysis, Chemometr. Intell. Lab. Syst. 2 (1987), https://doi.org/10.1016/0169-7439(87)80084-9.

[33] R.J. Barnes, M.S. Dhanoa, S.J. Lister, Standard normal variate transformation and de-trending of near-infrared diffuse reflectance spectra, Appl. Spectrosc. 43 (1989), https://doi.org/10.1366/0003702894202201.
[34] A. Savitzky, M.J.E. Golay, Smoothing and differentiation of data by simplified least squares procedures, Anal. Chem. 36 (1964), https://doi.org/10.1021/ac60214a047.
[35] Eigenvector Research, Classcenter, Eigenvector Research Documentation Wiki, 2013.
[36] S. Wold, A. Ruhe, H. Wold, W.J. Dunn III, The collinearity problem in linear regression. The partial least squares (PLS) approach to generalized inverses, SIAM J. Sci. Stat. Comput. 5 (1984), https://doi.org/10.1137/0905052.
[37] S. Wold, M. Sjöström, L. Eriksson, PLS-regression: a basic tool of chemometrics, in: Chemometrics and Intelligent Laboratory Systems, 2001, https://doi.org/10.1016/S0169-7439(01)00155-1.
[38] Eigenvector Research, Advanced Preprocessing: Sample Normalization, Eigenvector Research Documentation Wiki, 2021.
[39] A.A. Gowen, G. Downey, C. Esquerre, C.P. O'Donnell, Preventing over-fitting in PLS calibration models of near-infrared (NIR) spectroscopy data using regression coefficients, J. Chemom. 25 (2011), https://doi.org/10.1002/cem.1349.
[40] Eigenvector Research, Tools: Permutation Test, Eigenvector Research Documentation Wiki, 2014.
[41] H. van der Voet, Comparing the predictive accuracy of models using a simple randomization test, Chemometr. Intell. Lab. Syst. 25 (1994), https://doi.org/10.1016/0169-7439(94)85050-X.
[42] F. Castanedo, A review of data fusion techniques, Sci. World J. 2013 (2013), https://doi.org/10.1155/2013/704504.
[43] D.L. Hall, J. Llinas, An introduction to multisensor data fusion, Proc. IEEE 85 (1997), https://doi.org/10.1109/5.554205.
[44] F. Shihana, D.M. Dissanayake, N.A. Buckley, A.H. Dawson, A simple quantitative bedside test to determine methemoglobin, Ann. Emerg. Med. 55 (2010) 184–189, https://doi.org/10.1016/J.ANNEMERGMED.2009.07.022.
[45] A. Hofmann, A. Simon, T. Grkovic, M. Jones, UV-Vis spectroscopy, in: A. Hofmann, A. Simon, T. Grkovic, M. Jones (Eds.), Methods of Molecular Analysis in the Life Sciences, Cambridge University Press, Cambridge, 2014, pp. 15–37.
[46] Å. Rinnan, F. van den Berg, S.B. Engelsen, Review of the most common pre-processing techniques for near-infrared spectra, TrAC, Trends Anal. Chem. 28 (2009), https://doi.org/10.1016/j.trac.2009.07.007.
[47] M. Manley, Near-infrared spectroscopy and hyperspectral imaging: non-destructive analysis of biological materials, Chem. Soc. Rev. 43 (2014), https://doi.org/10.1039/c4cs00062e.
[48] G. Edelman, T.G. van Leeuwen, M.C.G. Aalders, Hyperspectral imaging for the age estimation of blood stains at the crime scene, Forensic Sci. Int. 223 (2012) 72–77, https://doi.org/10.1016/J.FORSCIINT.2012.08.003.
[49] B. Li, P. Beveridge, W.T. O'Hare, M. Islam, The estimation of the age of a blood stain using reflectance spectroscopy with a microspectrophotometer, spectral pre-processing and linear discriminant analysis, Forensic Sci. Int. 212 (2011) 198–204, https://doi.org/10.1016/J.FORSCIINT.2011.05.031.
[50] S. Willis, ENFSI guideline for evaluative reporting in forensic science - Strengthening the evaluation of forensic results across Europe, (STEOFRAE) (2015).
[51] A. Weber, A. Wójtowicz, I.K. Lednev, Post deposition aging of bloodstains probed by steady-state fluorescence spectroscopy, J Photochem Photobiol B 221 (2021). https://doi.org/10.1016/j.jphotobiol.2021.112251.
[52] S. Mc Shine, K. Suhling, A. Beavil, B. Daniel, N. Frascione, The applicability of fluorescence lifetime to determine the time since the deposition of biological stains, Analytical Methods 9 (2017). https://doi.org/10.1039/c6ay03099h.

PRACTICAL SUGGESTIONS FOR REAL CASE IMPLEMENTATION OF BLOODSTAIN DATING

Even though the approach involving data fusion provided the most accurate estimations of the age of bloodstains, it is evident that the simultaneous application of both spectroscopic methods may not always be feasible. For this reason, the final section of this article is dedicated to practical suggestion for bloodstain dating, starting from the methods of securing samples at the crime scene, up to the selection of the analytical method.

Evidence Collection: Before proceeding with any crime scene activities, proper documentation of the evidential bloodstains, including notation of their location, size, and characteristics, has to be ensured. At this stage, it will also be necessary to record the environmental conditions at the crime scene, including temperature, relative humidity, and the illumination of the sample with natural and artificial light sources. If possible, it is recommended to document these conditions in a daily cycle to enable the procedure of supervised aging [28]. In the case of revealing traces on non-absorbent substrates, secure the entire trace by isolating it from the substrate, trying to avoid complete disintegration of the evidence. Use a clean and dry collection tool to gather blood samples, avoiding contamination. In the case of revealing a trace on an absorbent substrate, if possible, it is advisable to secure the entire piece of evidence (when, for example, it constitutes a small or movable object). If this is not possible, do not use a moist cotton swab with a solution containing water, alcohol, or any other solvent that may lead to protein denaturation. In such a situation, it is recommended to cut/isolate the bloodstain along with a portion of the substrate. If this is also impossible, consider using portable spectrometers that allow spectrum recording at the crime scene.

Evidence Securing and Storing: Store collected bloodstains in airtight, light-resistant containers when dried (it is assumed that wet bloodstains will not be secured, as dating them is nonsensical). Do not use adhesive films (e.g., for securing microtraces), as the layer of adhesive present there can lead to contamination of the bloodstain. Maintain a consistent temperature and humidity – keep them as low as possible – to slow down degradation processes. Avoid sample irradiation with sunlight and artificial light sources. And finally try not to store the samples for an extended period, but to analyze them immediately after they are delivered to the laboratory. In this case, close collaboration with the police and forensic technicians is vital to raise awareness about the need for the prompt delivery of evidence materials for dating purposes.

Selection of Spectroscopic Method: Whenever possible (bloodstain easily separated from the substrate or absorbed onto light-colored material), it is recommended to use both research techniques – UV–Vis and NIR spectroscopies – operating in reflectance mode. Such an approach not only improves the accuracy of age estimation, as demonstrated in the present article, but also serves as a cross-verification element for the correctness of these estimations. When a bloodstain is deposited on an absorbing, dark-colored substrate, use NIR spectroscopy in reflectance mode. Avoid extracting samples from the substrate, as it may result in the “reversal” of the aging process and, consequently, an inaccurate estimation of the age of the bloodstain. Follow standard procedures for NIR and UV–Vis data

collection, establishing the parameters for obtaining good quality spectra depending on the nature of the sample (the substrate), according to inner procedures.

Validation and Reporting: Using a single universal regression model for dating traces is ineffective. The dating methodology should be tailored each time to the specific bloodstain, explicitly considering the conditions under which it underwent degradation. Details regarding this case-suited approach have been thoroughly discussed in [28][29]. Moreover, it is recommended to provide an evidence evaluation in the context of two contrasting hypotheses presenting different perspectives on the course of events, in this case concerning sample age. This aligns with the likelihood ratio (LR) approach-based reporting recommended by the European Network of Forensic Science Institutes (ENFSI) [50].

Continuous Learning and Collaboration: It is crucial to stay updated on spectroscopic techniques and forensic methodologies advancements. Moreover, in order to enhance the efficacy of bloodstain, it is mandatory as well to foster collaboration between practitioners and forensic scientists, especially those working on the development of novel spectroscopic tools for monitoring blood degradation. The proposed protocol should be expanded to include additional analytical methods, such as Raman [13,27] and fluorescence spectroscopies [51,52].

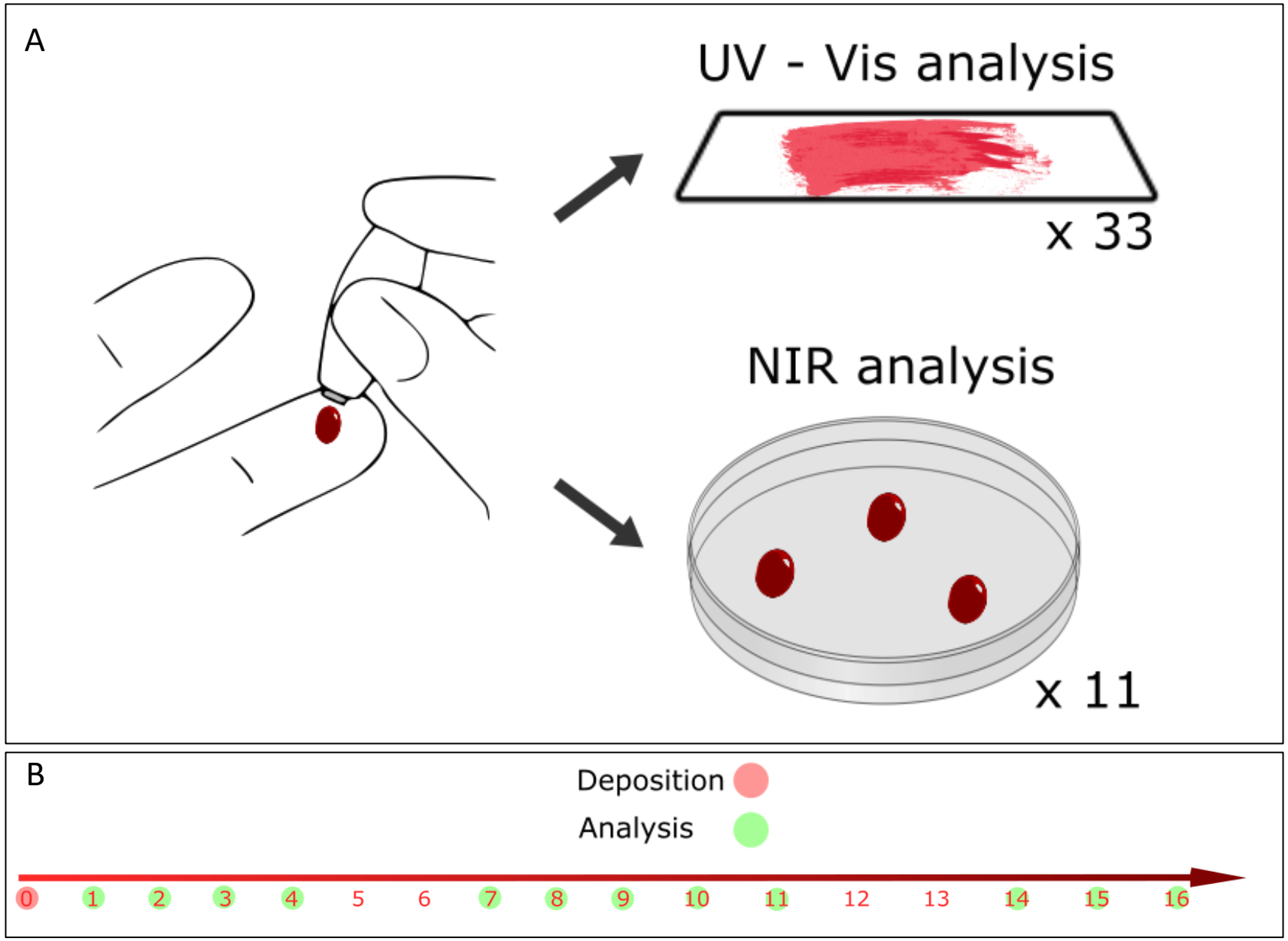

Figure S1: A: Visual schematization of sampling procedure, with indication of sample numerosity. B: Measurement scheme along time. A red circle indicates the day of sample deposition, while a green circle indicates a day during which samples were analysed.

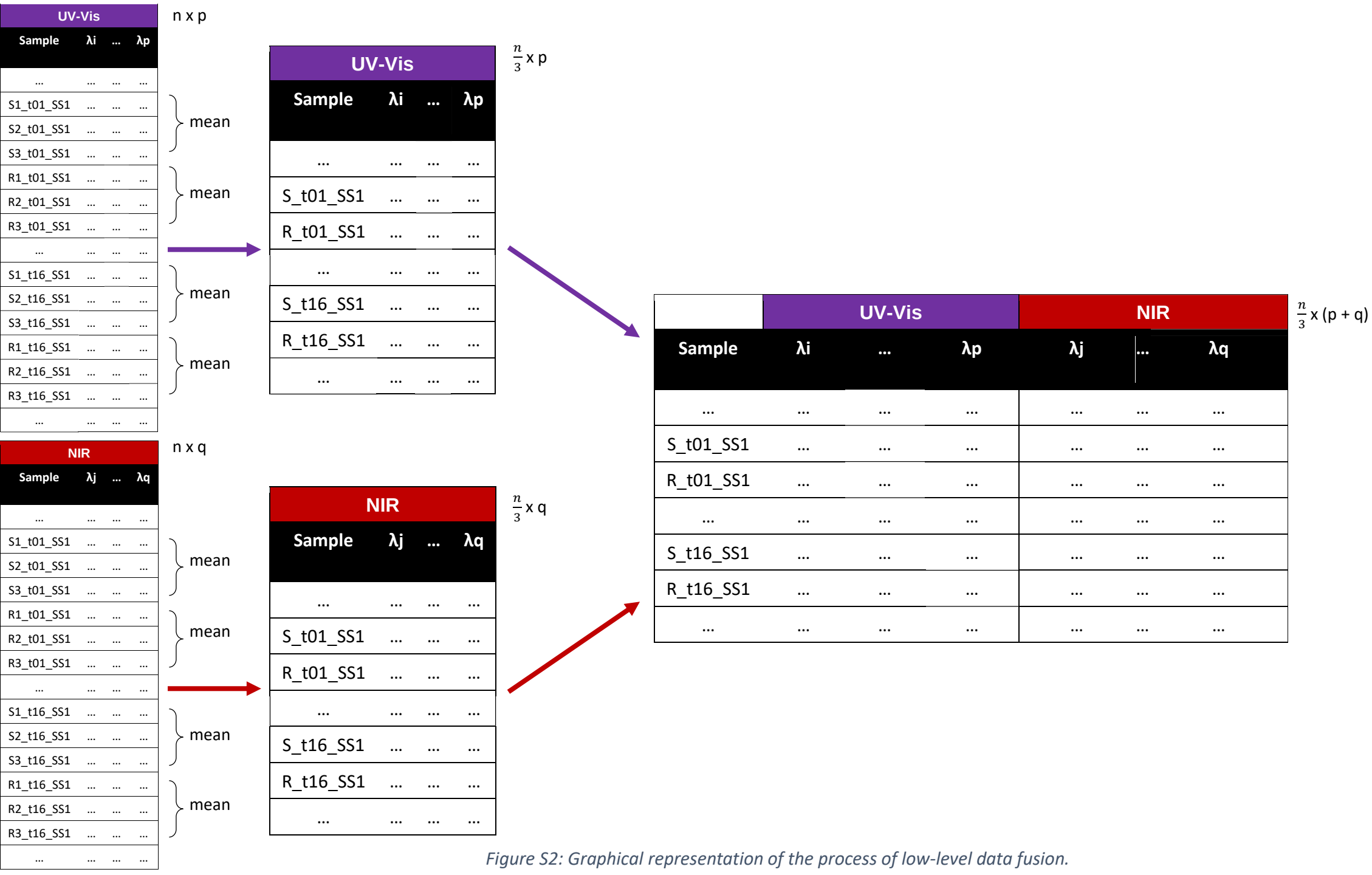

Figure S2: Graphical representation of the process of low-level data fusion.

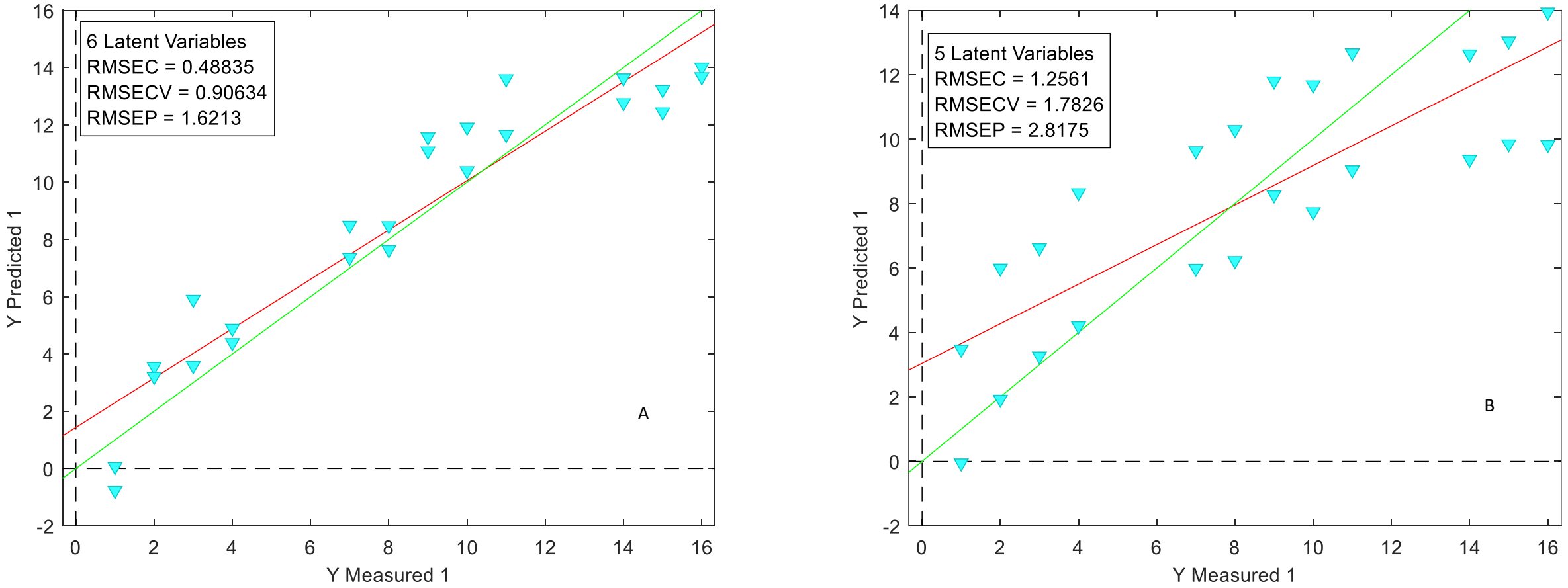

Figure S3: PLS-R models obtained from low level data fusion done with approach one (A) and two (B).